

R.I. Zapukhlyak¹, V.O. Kotsyubynsky¹, V.M. Boychuk¹, B.I. Rachiy¹, R.G. Abaszade^{2,3},
V.T. Hoi¹, M. Klymyuk¹

Structural Evolution of Porous Carbon Materials Derived from Hemp Fibers: Raman Spectroscopy Studies

¹Vasyl Stefanyk Precarpathian National University, Ivano-Frankivsk, Ukraine, volodymyr.kotsyubynsky@pnu.edu.ua

²Azerbaijan State Oil and Industry University, Baku, Azerbaijan, abaszada@gmail.com

³Azerbaijan University of Architecture and Construction, Baku, Azerbaijan

Raman spectroscopy was employed to investigate the structural evolution of porous carbon materials derived from hemp fibers through steam-assisted carbonization at temperatures of 400, 500, 600, 700, 800, and 900°C (K series), followed by nitric acid activation (KN series) and additional annealing in air (KNO series). The study is based on a comparison of the efficiency of two-component and five-component approximations for analyzing the 800-2000 cm⁻¹ spectral range in the Raman spectra of porous carbon. The two-component model, which describes only the D and G bands, provides a simplified assessment of graphitization and defect concentration, allowing for a quick evaluation of structural disorder by analyzing the ratio of the integrated intensities of the I_D and I_G spectral bands. The five-component approximation, incorporating the D₁, D₂, D₃, D₄, and G bands, offers a more detailed analysis of structural defects, significantly improving spectral fitting consistency (R² = 0.95-0.99) compared to the two-band model (R² = 0.80-0.88). A comparison of lateral crystallite size estimations using both approaches revealed a strong correlation between the obtained data (Pearson's r = 0.83-0.87) across all material series, confirming the reliability of the applied analytical methods. Additionally, the five-component model identified a correlation between the D₃ band position and crystallite size, a relationship that was not evident in the two-component approximation. These findings emphasize the effectiveness of the five-component deconvolution of Raman spectra for tracking structural transformations in carbon materials, providing additional insights crucial for material selection in energy storage, catalysis, and sorption applications.

Keywords: porous carbon material, carbonization, activation, Raman spectroscopy, secondary raw materials.

Received 03 September 2025; Accepted 11 February 2025.

Introduction

Porous carbon materials with a controllable structure are highly significant due to their unique physicochemical properties, including a tunable pore size, high surface area, and excellent electrical, thermal, and chemical stability [1,2,3]. These characteristics make them invaluable in applications such as energy storage, environmental remediation, catalysis, and biomedicine. The ability to tailor pore structures ranging from micropores (< 2 nm) for gas adsorption and molecular sieving, mesopores (2–50 nm) for improved mass transport, and macropores (>50 nm) for facilitating fast fluid flow –allows for optimization in various technological fields. Furthermore,

their synthesis from renewable sources, such as biomass, contributes to their sustainability, while scalable fabrication techniques, including templating, activation, and pyrolysis, facilitate industrial production [4,5]. The study of disordered porous carbons relies on a combination of experimental techniques to analyze their structural, textural, chemical, and electrochemical properties. Gas adsorption methods, such as nitrogen adsorption-desorption are employed to determine the specific surface area and pore size distribution. Electron microscopy techniques, including SEM and TEM, allow for direct visualization of the morphology and porosity of carbon materials. X-ray diffraction (XRD) is crucial for determining the degree of structural order in porous

carbons, differentiating between graphitic and amorphous carbon phases based on peak broadening. Small-angle X-ray scattering (SAXS) provide information on pore connectivity, fractal nature, and overall porosity. Each method provides complementary information, allowing for a comprehensive understanding of the material's porosity, structure, chemical composition, and functional performance in various applications. Spectroscopic methods offer valuable chemical and structural insights. Raman spectroscopy is a powerful technique for investigating porous carbon materials due to its ability to provide rapid, non-destructive, and detailed structural insights [6]. One of its primary advantages is its sensitivity to the degree of disorder and graphitization in carbon materials. Another key advantage of Raman spectroscopy is its ability to analyze porous carbon materials without requiring extensive sample preparation or complex vacuum environments [7]. Unlike techniques such as XRD, Raman spectroscopy can probe both crystalline and amorphous phases, making it particularly useful for characterizing disordered carbons. This is particularly valuable for applications in supercapacitors, batteries, and electrocatalysis, where structural evolution plays a crucial role in performance. Additionally, Raman spectroscopy is highly sensitive to functionalization and heteroatom doping (e.g., nitrogen, oxygen, or sulfur-doped carbons), which can modify electronic properties and catalytic activity.

I. Experimental details

Steam-assisted carbonization approach was used for obtaining of K- series of carbon materials [8]. Dry hemp fiber was mechanically ground and placed into a reactor, which was then filled with distilled water and placed in a furnace. The carbonization of the material was carried out in a water vapor atmosphere under a pressure of $8 \cdot 10^5$ Pa (pressure in the reaction medium was controlled through a regulated valve). Heating to the target temperature (400, 500, 600, 700, 800, 900 and 1000°C) was performed at a rate of 10°C/min. Once the desired temperature was reached, the material was held for 3 hours, after which the reactor was cooled down together with the heating system. Depending on the carbonization temperature, the resulting K-series samples were labeled as KX, where X represents the temperature at which carbonization was performed (e.g., K400 – material obtained by carbonizing hemp fibers at 400°C). Activation of the previously carbonized samples was carried out with nitric acid. The carbon materials were mixed with a 65% aqueous solution of HNO₃ in an 1:1 volume ratio. The mixture was kept for 3 hours under continuous stirring at the boiling temperature of the acid, after which the precipitate was washed with distilled water until the pH exceeded 5.0, followed by air drying at 65°C. The resulted samples were labeled as KNX (where X represents the temperature at which carbonization of origin material was performed) and formed KN series. Thermal treatment of previously nitric acid-activated samples was carried out in a vertical tubular furnace at 400°C in an air atmosphere for one hour. Obtained samples of KNO series were marked as KNOX, where X represents the carbonization temperature of

initial samples.

The study was conducted using a Horiba Jobin Yvon T-64000 Raman spectrometer, combined with an Olympus BX41 confocal microscope. A $\times 100$ objective with a numerical aperture of 0.09 was used, allowing for local beam focusing with a diameter of less than 1 μm , at a power of <10 mW. The Raman scattering was excited by Ar⁺/Kr⁺ laser radiation with a wavelength of 488 nm at room temperature in a backscattering geometry. The error in determining the position of the mode lines did not exceed 0.15 cm^{-1} .

II. Results and Discussion

The experimental spectra for the carbons obtained from hemp fibers after carbonization (K-series), after carbonization followed by nitric acid treatment (KN-series), and after carbonization, nitric acid treatment, and additional annealing at 400-1000°C (KNO-series) are presented in Fig. 1. The Raman spectra obtained for all studied carbon materials contain two peaks around 1580 cm^{-1} (G-mode) and 1350-1360 cm^{-1} (D-mode). The formation of the G-band results from the Raman scattering of light on doubly degenerate E_{2g}-symmetric vibrations of C-C bonds in sp²-hybridized carbon atoms. The presence of this band is a clear indication of carbon atoms forming graphitic fragments. Specifically, for pyrolytic graphite, the Raman spectrum consists of an intense G-band at 1580 cm^{-1} [9]. However, an increase in structural disorder leads to the appearance and increased relative intensity of the D-band. The D-band generally has a complex structure and is associated with π - π^* transitions, corresponding to the presence of sp²-hybridized carbon atoms. The relative intensity of the D-band increases with increasing structural disorder, [10]. The KNO-series materials, annealed at 700 and 800°C, exhibit a lack of structural ordering, as evidenced by the broadening of both the D and G bands, indicating that the material is in a state close to amorphous carbon. As a result of annealing at 900 and 1000°C, the material acquires a Raman spectrum typical for porous carbon. The complex composition of the Raman spectra of KNO-700 and KNO-800 samples is due to additional diffuse scattering of the optical signal in systems with a minimal size of scattering centers.

The ratio of the integrated intensities of the D and G peaks (I_D and I_G) can be used for assessing the degree of disorder of carbon material—higher values indicate a greater number of structural defects. According to the of [10], the average size L_R (nm) of graphite crystallites in the direction parallel to the (002) basal plane can be empirically related to I_D/I_G through the following equation:

$$L_{2R}(nm) = (2.4 \times 10^{-10})\lambda^4(I_G/I_D)$$

where λ (nm) is the wavelength of the excitation laser radiation. There are two main approaches for analyzing the Raman spectra of carbon materials. In several studies, [11,12,13] the analysis of Raman spectra of carbon materials considers only two components: the G and D bands. This approach provides a simplified yet effective way to assess structural disorder and graphitization by

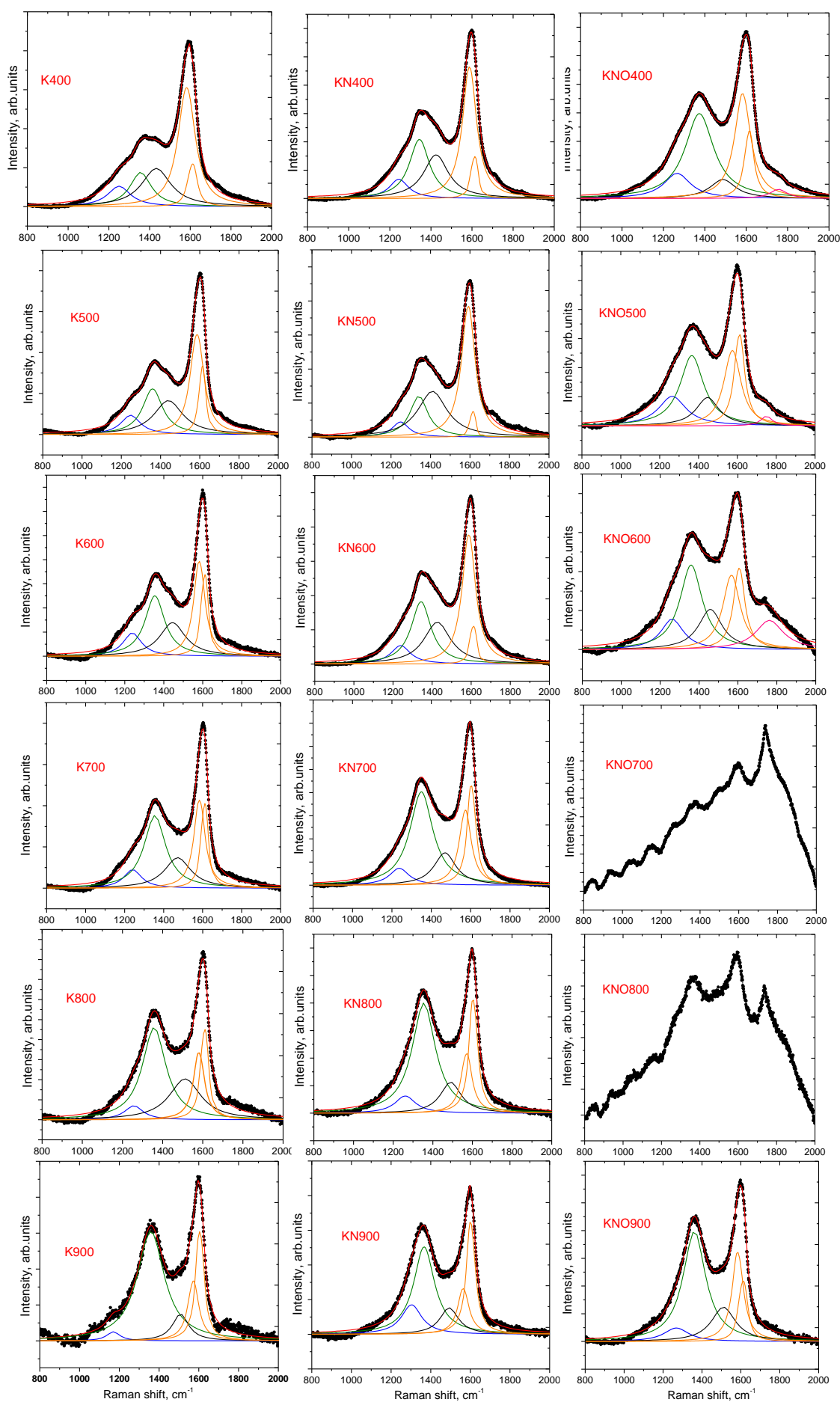


Fig. 1. Raman spectra of carbon materials of the K, KN, and KNO series.

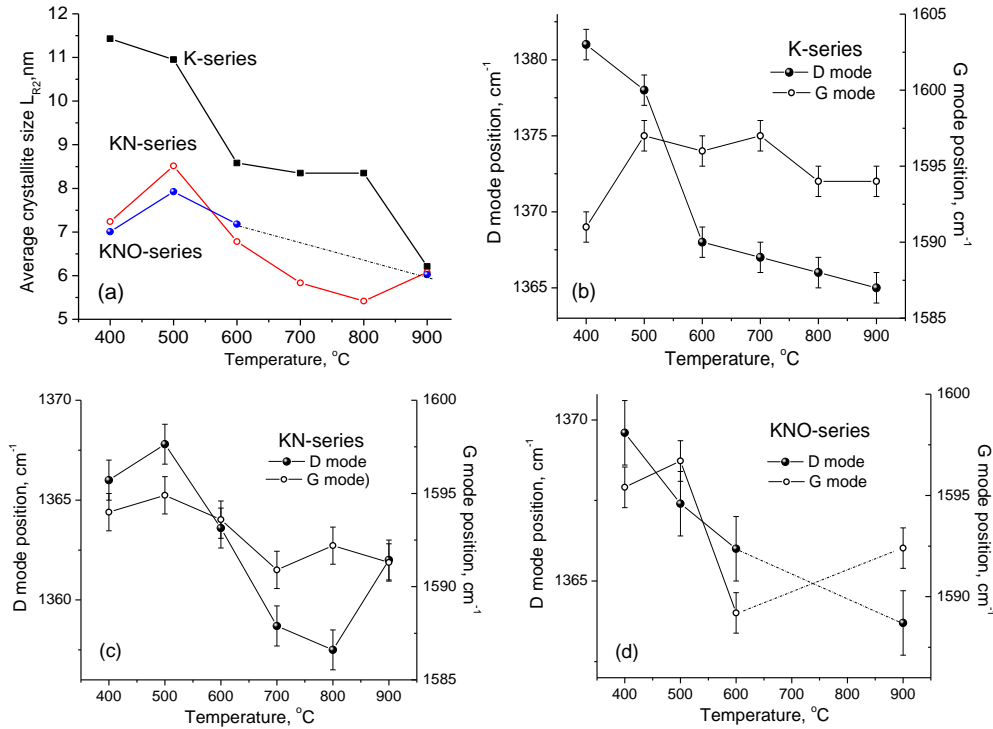


Fig. 2. (a) Lateral crystallite sizes of graphite as a function of the carbonization temperature of the raw material; the position of the D and G bands in the Raman spectra of carbon materials of the (b) K-, (c) KN-, and (d) KNO-series (calculation based on the two-component approximation).

focusing on the main vibrational modes of sp^2 -hybridized carbon (G-band) and defect-induced scattering (D-band). Other researchers, including [14,15,16], adopt a more detailed approach by using a five-component approximation. This method accounts for the complexity of disordered carbon structures and provides a more accurate description of different defect types and local structural variations. The five-band model typically includes: D_1 ($\sim 1350\text{ cm}^{-1}$) - associated with disordered graphitic structures and sp^3 carbon defects; D_2 ($\sim 1620\text{ cm}^{-1}$) - related to disordered graphitic edges or amorphous carbon; D_3 ($\sim 1500\text{ cm}^{-1}$) - attributed to amorphous carbon contributions; D_4 ($\sim 1200\text{ cm}^{-1}$) - related to sp^2 - sp^3 hybridized structures; G ($\sim 1580\text{ cm}^{-1}$) - corresponding to graphitic domains.

The choice between two-band and five-band approximation depends on the level of structural complexity and the research objectives. While the simpler two-band model is useful for a quick assessment of

graphitization and defect concentration, the five-band model provides deeper insight into defect types, amorphous contributions, and different bonding environments, making it particularly useful for highly disordered porous carbons. To identify general trends and correlations between spectral parameters and the structural characteristics of the materials, both spectral fitting approaches were tested: two-component approximation and five-component approximation using Lorentzian functions. The coefficient of determination (R^2), which quantifies the proportion of experimental data that aligns with the applied model, ranged from 0.80 to 0.88 when using the two-component model. In contrast, when the five-component model was applied, R^2 increased to 0.95-0.99, indicating a significantly better fit. For the five-component approximation the calculation of the lateral crystallite sizes L_{R5} was performed using the following relationship:

$$L_{5R}(nm) = (2.4 \times 10^{-10})\lambda^4 \left(\frac{I_G + I_{D2}}{I_{D1} + I_{D3} + I_{D4}} \right)^{-1}$$

This approach provides a more precise assessment of crystallite size variations in highly disordered carbon structures by accounting for multiple defect-related components in the Raman spectrum.

The calculation based on two-component approximation (Fig.2a) show that lateral crystallite size for K-series carbons decreases in a range of 11.5-6.3 nm with carbonization temperature growth indicating material fragmentation. The similar behavior is observed for KN-

series samples only changes occur in the range of 8.5-5.5 nm. The smallest change in L_{R2} in the range of about 7-6 nm was observed for the KNO system. As the carbonization temperature increased the D-band shifted toward lower frequencies, which is associated with dispersion-related vibrations in the defective graphite lattice (Fig.2b). This shift can be interpreted as a reduction in local structural stresses that influence C-C bond vibration energies. After thermal treatment, as the

structure of carbon fragments recovers, the D-band shifts further to lower frequencies, indicating a decrease in defect density. The G-band also exhibited a slight shift from $\sim 1600\text{ cm}^{-1}$ to $\sim 1595\text{ cm}^{-1}$, which can be attributed to the relaxation of micro-stresses in the graphite-like structure. For the KN-series, the D-band reached a minimum position for the sample carbonized at 800°C , followed by a reverse shift at higher temperatures (Fig. 2c). The G-band shifted from 1595 cm^{-1} to 1590 cm^{-1} , showing a trend similar to that observed for the K-series. This suggests that acid treatment is most effective for materials obtained by carbonization in the $700\text{-}800^\circ\text{C}$ range. Similar trends were observed for the KNO-series (Fig. 2d). A correlation between the D-mode position and the lateral crystallite size was observed (Fig. 2e) for all series. In the K- and KN-series, a linear relationship was observed between the D-band position and lateral crystallite size (L_{R2}) with Pearson correlation coefficients of 0.94 and 0.95, respectively. The variation in parameters for KNO series can be explained by both the smaller number of experimental values and the narrower range of D-mode position variation due to only minor changes in graphite crystallite sizes. This is the first time that a correlation between the D-band position and structural characteristics of carbon materials has been observed and documented.

The dependence of lateral crystallite sizes of graphite (L_{R5}) on carbonization temperature for the K-, KN-, and KNO-series materials, calculated using the five-component approximation, is highly similar to the results obtained using the two-component approximation. Across all systems, a general trend of decreasing lateral crystallite sizes is observed within the carbonization temperature range of $400\text{-}900^\circ\text{C}$ (Fig. 3a). The smallest variation of

L_{R5} in the range of 9-6 nm was recorded for the KNO system. Three characteristic temperature regions can be distinguished, corresponding to structural transitions: $400\text{-}500^\circ\text{C}$ (I), $600\text{-}800^\circ\text{C}$ (II) and $800\text{-}900^\circ\text{C}$ (III) corresponding to different rates of crystallite size change. For the K-series samples, regions I and II merge into one, showing a rapid decrease in crystallite sizes from 14.0 nm to 5.3 nm for samples thermally treated within $400\text{-}800^\circ\text{C}$. Beyond this range, the crystallite size begins to increase, reaching 6.5 nm for K1000. In K900, the graphite crystallite size reduces to 6 nm, followed by growth to 7 nm at 1000°C , which is attributed to the onset of graphitization processes. For KN400, the average lateral crystallite size is approximately 11 nm, which can be explained by material fragmentation due to acid treatment. However, for other KN-series samples, the crystallite sizes are 5-10% larger compared to the K-series materials, likely due to the "washing out" of smaller particles during HNO_3 treatment. The crystallite size variations in the KNO-series follow a similar trend as the K and KN-series, but with generally smaller lateral crystallite sizes, particularly at 400°C , where the size is 8.8 nm. A correlation was observed between the lateral crystallite sizes and the inverse ratio of the integrated intensity of the D_1 mode to the sum of the intensities of the G and D_2 modes.

The changes in the integrated intensity of spectral components for all systems exhibit a complex pattern. There is a clear trend of increasing relative intensity of the D_1 component up to $800\text{-}900^\circ\text{C}$, followed by a decline at higher temperatures (Fig. 3b). This behavior can be explained by the decrease in the relative content of the disordered graphite lattice fraction at 900°C , due to particle sintering and growth.

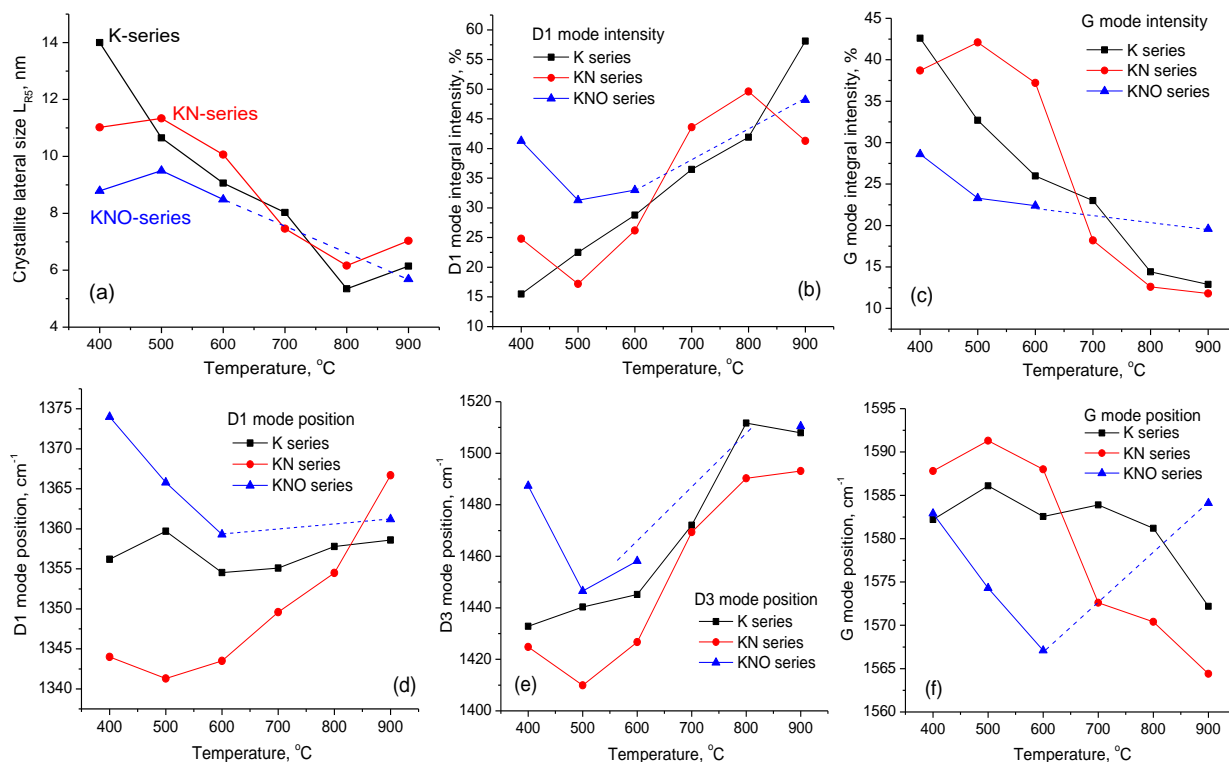


Fig. 3. (a): Lateral crystallite sizes of graphite as a function of the carbonization temperature of the precursor materials, integral intensities of (b) D1 mode, (c) G mode, the positions of the (d) D1, (e) D3 and (f) G bands in the Raman spectra of carbon materials of the K, KN, and KNO series (calculation based on the five-component).

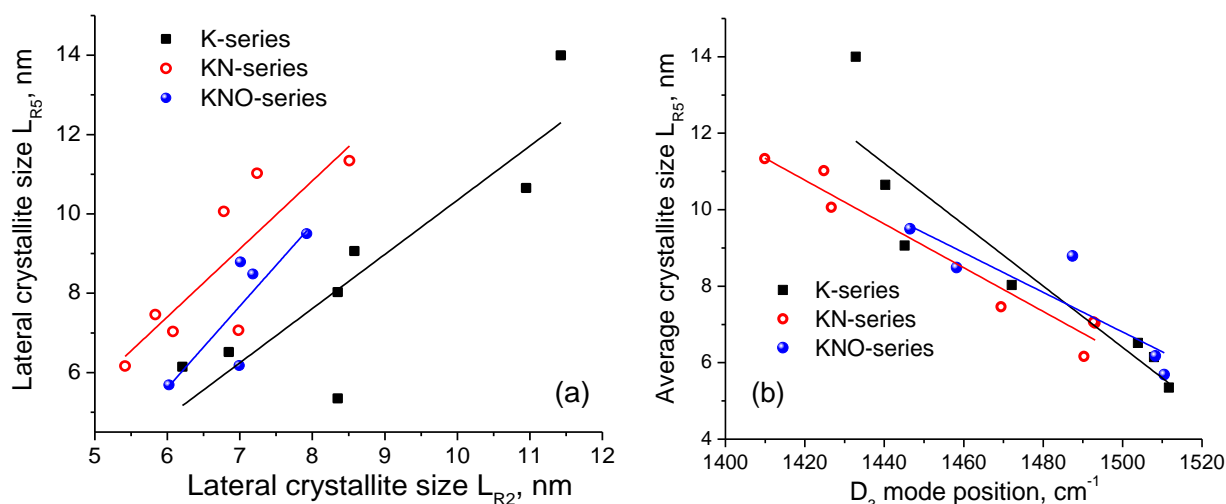


Fig. 4. Correlation fields between (a) lateral sizes of crystallites L_{R2} and L_{R5} , (b) lateral size L_{R5} and the positions of D_3 modes for carbon materials of K-, KN- and KNO-series.

Conversely, the change in the integrated intensity of the G-mode follows a mirrored trend (Fig. 3c). As the relative intensity of the D_1 band increases, indicating a higher degree of disorder, the G-mode intensity decreases, reflecting a reduction in graphitic ordering. At higher temperatures the trend reverses, suggesting an improvement in structural ordering due to graphitization and particle coalescence.

A positive shift in the D_1 mode position in the Raman spectra of K and KN carbons is observed simultaneously with a negative shift in the G-mode position in these systems (Fig. 3d). However, for the KNO-series materials, which underwent additional annealing in air, no such trends were detected. In the KN-series, the Raman shift of the D_1 mode reaches a maximum at 900°C , corresponding to the minimum position of the G-mode (Fig. 3d-3f). The D_1 band in Raman spectra of carbon materials results from a two-phonon process in defective structures formed by sp^2 -hybridized carbon atoms. This band is associated with localized defects, such as dislocations, vacancies, functional groups, or edge regions of graphene sheets. The observed behavior of the D_1 mode- an initial negative shift followed by a positive shift- corresponds to an increase in material disorder. The D_3 band, which is associated with the amorphous fraction of carbon materials, represents regions without a clearly defined graphitic or ordered sp^2 structure and is linked to C-C bond vibrations in disordered environments (Fig. 3e). The shift of the D_3 band in Raman spectra serves as an indicator of structural and chemical changes in amorphous carbon materials. Experimentally, the positive shift in the D_3 band, with saturation at 800 - 900°C , is associated with increased vibrational dispersion in chaotically ordered regions, indicating increased amorphization. Additionally, mechanical stress in the structure can cause a D_3 shift to higher frequencies, as it alters the local vibrational energy of sp^2 bonds. The D_2 band arises from a dispersion process similar to the main D_1 band but differs in its generation mechanism, appearing as a shoulder on the G-band. In graphite-like materials, the presence of the D_2 band is linked to smaller lateral crystallite sizes. In samples with larger crystallites, the intensity of the D_2 band decreases.

Across all material systems, a consistent shift in the positions of the G and D_2 bands is observed, showing a typical trend toward a negative shift.

A positive correlation between the G- and D_2 -mode positions was found for all materials, with Pearson correlation coefficients of 0.95, 0.99, and 0.74 for the K-, KN-, and KNO-series, respectively. This correlation confirms the validity of the spectral deconvolution into individual components. Analyzing the dynamics of spectral component shifts with increasing carbonization temperature, it can be noted that D_3 and D_4 positions are the most sensitive parameters. This reflects changes in the relative content of surface functional groups (D_3) and the degree of lattice disorder and/or the presence of sp -hybridized carbon atoms (D_4). A similar conclusion can be drawn from the analysis of line width variations, where the maximum variation is observed for the D_3 and D_4 components, further emphasizing their sensitivity to processing conditions.

A strong positive correlation was observed between L_{R2} and L_{R5} , with Pearson correlation coefficients of 0.87, 0.83, and 0.83 for the K, KN, and KNO systems, respectively (Fig. 4a). However, the expected relationship between L_{R5} and the position of the D_1 mode was not detected. Instead, a linear correlation was found between L_{R5} for all three material systems and the position of the D_3 mode (Fig. 4b). This correlation can be explained as follows: the shift of the D_3 band to higher frequencies occurs when the content of amorphous carbon increases, which in turn corresponds to a decrease in crystallite size. This is the first experimental confirmation of a relationship between lateral crystallite sizes of graphitic domains in plant-derived porous carbon and the position of the D_3 mode in the Raman spectrum.

Conclusions

This study is based on the Raman investigation of hemp fiber-derived porous carbon materials synthesized using steam-assisted carbonization (K series), nitric acid activation (KN series) and additional annealing (KNO

series). The comparison between the two-component and five-component approximations in the analysis of characteristic region (800-2000 cm^{-1}) of Raman spectra of porous carbons. The two-component model, which considers only the D and G bands, provides a simplified but effective method for assessing graphitization and defect concentration. It allows for a quick estimation of the degree of disorder through the I_D/I_G ratio and offers a straightforward approach to evaluating the structural properties of carbons. However, this method lacks the resolution needed to fully capture complex defect structures, amorphous contributions, and variations in local bonding environments. In contrast, the five-component approximation, which includes D_1 , D_2 , D_3 , D_4 , and G bands, provides a more detailed and accurate description of the disorder within carbon materials. The five-band model demonstrated a significantly improved fit to the experimental data, with R^2 values increasing from 0.80-0.88 (two-band model) to 0.95-0.99 (five-band model), confirming its ability to describe structural heterogeneity. The comparison of lateral crystallite size estimations (L_{R2} vs. L_{R5}) highlights the differences between the two models. A strong correlation (Pearson's

$r = 0.87-0.83$) was observed between L_{R2} (two-band model) and L_{R5} (five-band model) across the K-, KN-, and KNO-series, confirming that both methods are consistent in detecting crystallite size trends. However, the five-band model provided a more refined differentiation between graphitic, amorphous, and defective carbon regions, making it particularly useful for studying highly disordered porous carbons. Additionally, the five-component model revealed new correlations between Raman spectral features and structural parameters, such as the relationship between D_3 band position and crystallite size, which was not apparent in the two-component approximation.

Zapukhlyak R.I. – PhD, Associate Professor;
Kotsyubynsky V.O. – Professor, Doctor of Sciences;
Boychuk V.M. – Professor, Doctor of Sciences;
Rachiy B.I. – Professor, Doctor of Sciences;
Abaszade R.G. – PhD, Associate Professor;
Hoi– V.T. – PhD student;
Klymyuk M.M. – PhD student.

- [1] M. Ni, L. Zhou, Y. Liu, R. Ni *Advances in the synthesis and applications of porous carbon materials*, *Frontiers in Chemistry*, 11, 1205280 (2023); <https://doi.org/10.3389/fchem.2023.1205280>.
- [2] Z. Pan, S. Yu, L. Wang, C. Li, F. Meng, N. Wang, Y. Zhang. *Recent advances in porous carbon materials as electrodes for supercapacitors*, *Nanomaterials*, 13(11), 1744 (2023); <https://doi.org/10.3390/nano13111744>.
- [3] V. Boychuk, V. Kotsyubynsky, A. Kachmar, S. Budzulyak, I. Budzulyak, B. Rachiy, L. Yablon, *Effect of Synthesis Conditions on Pseudocapacitance Properties of Nitrogen-Doped Porous Carbon Materials*, *Journal of Nano Research*, 59, 112(2019); <https://doi.org/10.4028/www.scientific.net/JNanoR.59.112>.
- [4] L. Sun, Y. Gong, D. Li, C. Pan, *Biomass-derived porous carbon materials: synthesis, designing, and applications for supercapacitors*, *Green Chemistry*, 24(10), 3864 (2022); <https://doi.org/10.1039/D2GC00099G>.
- [5] B.K. Ostafiychuk, R.P. Lisovskiy, A.H.Z. Al-Saedi, B.I. Rachiy, V.O. Kotsyubynsky, P.I. Kolkovsky, A.B. Hrubciak *Effect of orthophosphoric acid on morphology of nanoporous carbon materials*, *Journal of Nano and Electronic Physics*, 11(3), 03036-1 (2019); [https://doi.org/10.21272/jnep.11\(3\).03036](https://doi.org/10.21272/jnep.11(3).03036).
- [6] H.M. Heise, R. Kuckuk, A.K. Ojha, A. Srivastava, V. Srivastava, B.P. Asthana *Characterisation of carbonaceous materials using Raman spectroscopy: a comparison of carbon nanotube filters, single and multi-walled nanotubes, graphitised porous carbon and graphite*, *Journal of Raman Spectroscopy: An International Journal for Original Work in all Aspects of Raman Spectroscopy, Including Higher Order Processes, and also Brillouin and Rayleigh Scattering*, 40(3), 344 (2009); <https://doi.org/10.1002/jrs.2120>.
- [7] G. Lipinski, K. Jeong, K. Moritz, M. Petermann, E. F. May, P. L. Stanwix, M. Richter *Application of Raman Spectroscopy for Sorption Analysis of Functionalized Porous Materials*, *Advanced Science*, 9(9), 2105477 (2022); <https://doi.org/10.1002/advs.202105477>.
- [8] V. Kotsyubynsky, B. Rachiy, V. Boychuk, I. Budzulyak, L. Turovska, M. Hodlevska *Correlation between structural properties and electrical conductivity of porous carbon derived from hemp bast fiber*, *Fullerenes, Nanotubes and Carbon Nanostructures*, 30(8), 873 (2022); <https://doi.org/10.1080/1536383X.2022.2033729>.
- [9] L.G. Cancado, M.A. Pimenta, B.R. A. Neves, M.S. S. Dantas, A. Jorio *Influence of the atomic structure on the Raman spectra of graphite edges*, *Physical review letters*, 93(24), 247401 (2004); <https://doi.org/10.1103/PhysRevLett.93.247401>.
- [10] M.A. Pimenta, G. Dresselhaus, M. S. Dresselhaus, L. G. Cancado *Studying disorder in graphite-based systems by Raman spectroscopy*, *Phys.Chem.Chem.Phys.* 9(11), 1276 (2007); <https://doi.org/10.1039/B613962K>.
- [11] X. Zeng, S. Yu, L. Ye, M. Li, Z. Pan, R. Sun, J. Xu *Encapsulating carbon nanotubes with SiO₂: a strategy for applying them in polymer nanocomposites with high mechanical strength and electrical insulation*, *Journal of Materials Chemistry C*, 3(1), 187 (2015); <https://doi.org/10.1039/C4TC01051E>.
- [12] V. Eswaraiah, V. Sankaranarayanan, S. Ramaprabhu *Inorganic nanotubes reinforced polyvinylidene fluoride composites as low-cost electromagnetic interference shielding materials*. *Nanoscale research letters*, 6, 1 (2011); <https://doi.org/10.1186/1556-276X-6-137>.
- [13] V. Duc Chinh, G. Speranza, C. Migliaresi, N. Van Chuc, V. Minh Tan, N.T. Phuong *Synthesis of gold nanoparticles decorated with multiwalled carbon nanotubes (Au-MWCNTs) via cysteaminium chloride functionalization*, *Scientific reports*, 9(1), 5667 (2019); <https://doi.org/10.1038/s41598-019-42055-7>.

- [14] S. Breitenbach, C. Unterweger, A. Lumetzberger, J. Duchoslav, D. Stifter, A. W. Hassel, C. Fürst *Viscose-based porous carbon fibers: improving yield and porosity through optimization of the carbonization process by design of experiment*, Journal of Porous Materials, 28, 727 (2021); <https://doi.org/10.1007/s10934-020-01026-4>.
- [15] A. Y. Lee, K. Yang, N. D. Anh, C. Park, S. M. Lee, T.G. Lee, M. S. Jeong *Raman study of D* band in graphene oxide and its correlation with reduction*, Applied surface science, 536, 147990 (2021); <https://doi.org/10.1016/j.apsusc.2020.147990>.
- [16] Z. Liu, D. Cao, G. Chen, Z. Bi, Q. Chen *Experimental Verification for the Graphitization of Inertinite*, Minerals, 13(7), 888 (2023); <https://doi.org/10.3390/min13070888>.

Р.І. Запухляк¹, В.О. Коцюбинський¹, В.М. Бойчук¹, Б.І. Рачій¹, Р.Г. Абсазаде^{2,3},
В.Т. Гой¹, М.М. Клим'юк¹

Структурні властивості пористого вуглецю, отриманого з волокон коноплі: порівняльне дослідження апроксимацій раманівських спектрів

¹Прикарпатський національний університет імені Василя Стефаника, Івано-Франківськ, Україна
volodymyr.kotsyubynsky@pnu.edu.ua

²Азербайджанський державний університет нафти і промисловості, Баку, Азербайджан, abaszada@gmail.com

³ Азербайджанський університет архітектури і будівництва, Баку, Азербайджан

Раманівська спектроскопія застосована для дослідження еволюції структури пористих вуглецевих матеріалів отриманих з волокон коноплі методом стимульованої парою карбонізації при температурах 400, 500, 600, 700, 800, та 900 (серія К) з наступною активацією азотною кислотою (серія KN) та за умови додаткового відпалу на повітрі (серія KNO). Дослідження ґрунтується на порівнянні ефективності застосування двокомпонентної та п'ятикомпонентної апроксимації для аналізу спектрального діапазону 800-2000 см⁻¹ у спектрах Рамана пористого вуглецю. Двокомпонентна модель, що описує лише D- та G-смуги, дозволяє спрощено оцінювати ступінь графітизації та концентрацію дефектів, надаючи можливості швидкої оцінки рівня структурного розпорядкування через аналіз відношення інтегральної інтенсивностей спектральних смуг I_D та I_G. П'ятикомпонентна апроксимація, яка включає D₁, D₂, D₃, D₄ та G-смуги, забезпечує детальніший аналіз структурних дефектів, покращуючи покращила узгодженість спектрального підбору (R² = 0.95-0.99) порівняно з двосмуговою моделлю (R² = 0.80-0.88). Порівняння оцінок латеральних розмірів кристалітів з використанням обох підходів виявило сильну кореляцію між отриманими даними (коефіцієнт Пірсона r=0.83-0.87) для всіх серій матеріалів, що підтверджує достовірність застосованих підходів до аналізу експериментальних даних. Водночас, п'ятикомпонентна модель виявила кореляцію між положенням D₃-смуги та розміром кристалітів, яка не була очевидною в двокомпонентній апроксимації. Ці результати підкреслюють ефективність п'ятикомпонентної деконволюції спектрів Рамана для відстеження структурних трансформацій у вуглецевих матеріалах, що надає додаткові результати, важливі при підборі матеріалів для застосувань у галузях накопичення енергії, каталізу та сорбції.

Ключові слова: пористий вуглецевий матеріал, карбонізація, активація, раманівська спектроскопія, вторинна сировина.